

RE-VISIT OF HST FUV OBSERVATIONS OF HOT-JUPITER SYSTEM HD 209458: NO SIII DETECTION AND THE NEED FOR COS TRANSIT OBSERVATIONS

G. E. BALLESTER

University of Arizona, Dept. of Planetary Sciences, Lunar & Planetary Laboratory,
1541 E University Blvd., Tucson, AZ 85721-0063 USA

AND

L. BEN-JAFFEL¹

UPMC Univ Paris 06, UMR7095, Institut d'Astrophysique de Paris, F-75014 Paris, France

Draft version February 19, 2018

ABSTRACT

The discovery of O I atoms and C II ions in the upper atmosphere of HD 209458b, made with the Hubble Space Telescope Imaging Spectrograph (STIS) using the G140L grating, showed that these heavy species fill an area comparable to the planet's Roche lobe. The derived $\sim 10\%$ transit absorption depths require super-thermal processes and/or supersolar abundances. From subsequent Cosmic Origins Spectrograph (COS) observations, C II absorption was reported with tentative velocity signatures, and absorption by Si III ions was also claimed in disagreement with a negative STIS G140L detection. Here, we revisit the COS dataset showing a severe limitation in the published results from having contrasted the in-transit spectrum against a stellar spectrum averaged from separate observations, at planetary phases 0.27, 0.72, and 0.49. We find variable stellar Si III and C II emissions that were significantly depressed not only during transit but also at phase 0.27 compared to phases 0.72 and 0.49. Their respective off-transit 7.5 and 3.1% flux variations are large compared to their reported $8.2 \pm 1.4\%$ and $7.8 \pm 1.3\%$ transit absorptions. Significant variations also appear in the stellar line shapes, questioning reported velocity signatures. We furthermore present archive STIS G140M transit data consistent with no Si III absorption, with a negative result of 1.7 ± 18.7 including $\sim 15\%$ variability. Silicon may still be present at lower ionization states, in parallel with the recent detection of extended magnesium, as Mg I atoms. In this frame, the firm detection of O I and C II implying solar or supersolar abundances contradicts the recent inference of potential $\times 20$ – 125 subsolar metallicity for HD 209458b.

Subject headings: planetary systems – stars: individual: HD 209458 – ultraviolet: stars – techniques: spectroscopic – planets and satellites: atmospheres

1. INTRODUCTION

UV detection of both hydrogen and heavy species on the extended atmospheres of hot exoplanets orbiting inside 0.1 AU from their stars provides a useful tool for understanding the properties of these uppermost planetary layers, the energy input from the immense stellar X-ray and UV (XUV) radiation and the processes of interaction with the incident stellar wind magnetized plasma. Provided information on the velocity distribution can be estimated in the transmission signature, the relative abundance of heavy species can be constrained to in turn reveal compositional properties that also pertain to the lower atmosphere and nature of the exoplanet. UV studies of exoplanets can thus provide unique information for their characterization that is usually unaccessible with IR and optical observations. Most of what we understand about hot-Jupiter upper atmospheres is based on far-ultraviolet (FUV) *Hubble Space Telescope* (*HST*) transit observations and extensive modeling of HD 209458b, which orbits a G0V star at 0.047 AU. However, as we show in this paper, the full *HST* FUV observational potential of this target has yet to be reached.

Using the Space Telescope Imaging Spectrograph (STIS) with the G140M medium-resolution ($R \sim 10,000$) grating, a $\sim 10\%$ absorption in Lyman- α was discovered by HI atoms in an inflated atmosphere reaching the Roche lobe distance of $\sim 2.9 R_{pl}$ (Vidal-Madjar et al. 2003, 2008; Ben-Jaffel 2007, 2008). A Lyman- α absorption with an enhanced blue-shifted component was first reported from the average of three medium-resolution G140M transits by Vidal-Madjar et al. (2003), while Ben-Jaffel (2008), who included a fourth partial transit, found a more symmetric average absorption in the red and blue wings. Existing theoretical models have tried to reproduce the HI observations assuming the solar XUV input where the atmospheric inflation results from heating at the base of the thermosphere around 0.01 – $1 \mu\text{bar}$, yielding a mean temperature of order $10,000$ K that drives a hydrodynamic outflow. Most models find enough thermal atomic hydrogen to reproduce the symmetric absorption profile originally reported in Ben-Jaffel (2008) for the HD 209458b transits (Ben-Jaffel 2008; Ben-Jaffel & Hosseini 2010; Trammell et al. 2011; Koskinen et al. 2010, 2013a). However, some issues remain unresolved regarding the exact total thermal H content that depends on the atmospheric solar or supersolar abundances assumed (Ben-Jaffel & Hosseini 2010; Koskinen et al. 2010, 2013a,b), on the strength of the outflow and the tidal effects (e.g., Lammer et al.

gilda@lpl.arizona.edu
bjaffel@iap.fr

¹ Visiting Research Scientist, University of Arizona, Lunar & Planetary Laboratory.

2003; Yelle 2004; Tian et al. 2005; García Muñoz 2007; Murray-Clay et al. 2009; Stone & Proga 2009; Guo 2011, 2013; Bourrier et al. 2014), on the geometrical distribution of the gas which can be global or quite likely confined at low (magnetic) latitudes due to the presence of a planetary magnetic field (Trammell et al. 2011, 2014; Adams 2011; Khodachenko et al. 2012; Cohen & Gloer 2012; Owen & Adams 2014), as well as on the presence of non-thermal processes affecting the energetics and line broadening (Ben-Jaffel & Hosseini 2010), and on the strength of the stellar XUV heating (Ballester et al. 2015). Charge exchange with the incident stellar wind protons (Holmström et al. 2008; Tremblin & Chiang 2013; Bourrier & Lecavelier 2013) and stellar radiation pressure (Vidal-Madjar et al. 2003) are also key mechanisms that predict an asymmetric Lyman- α transit absorption profile, but the relevance of these processes depends on the inclusion of natural line broadening (Ben-Jaffel 2008) and self-shielding (Bourrier & Lecavelier 2013), and a comprehensive analysis is required including the presence of a planetary magnetic field (Kislyakova et al. 2014) and the inherent absorption by the interstellar medium that may erase the asymmetric absorption feature if the Doppler shift is not strong enough. Probably the interstellar medium (ISM) absorption and the relatively low signal-to-noise ratio (S/N) limit the HI Lyman- α data analysis and interpretation, yet all studies agree on the important result that an area equivalent to the size of the Roche lobe is filled on HD 209458b, a finding that has many implications on our understanding of these atmospheres when connected with transit signatures in other species (Ben-Jaffel & Hosseini 2010). However, we must stress here that available observations already show that we are close to making a final diagnostic on the very nature of the transit absorption as shown by the comparison between light curves derived for the blue and red wings of the HI Lyman- α line (e.g., Fig. 3 in Ben-Jaffel 2008). For the relatively good signal to noise reported thus far (Ben-Jaffel 2008), repeated new STIS G140M medium-resolution transit observations of HD 209458b should help converge our determination of the HI Lyman- α transit absorption profile for this planet, and definitely elucidate any asymmetric spectral absorption signature. Additionally, time variation may be present in the HI Lyman- α spectral signature of HD 209458b, as can be seen in Fig. 3b of (Ben-Jaffel 2007). Similarly, time variation has been clearly identified in the HI Lyman- α absorption of the hot-Jupiter HD 189733b (Lecavelier et al. 2012; Bourrier et al. 2013). On HD 189733b, one STIS observation showed no HI Lyman- α absorption while on another date it showed absorption that was enhanced in the blue wing. A STIS observation of GJ 436b has also shown an extended hydrogen atmosphere on this warm Neptune, revealing a post-egress signature from a hydrogen tail with an enhanced blue-shifted HI Lyman- α absorption (Kulow et al. 2014).

On HD 209458b, the STIS detection of extended neutral oxygen atoms and singly ionized carbon (the two dominant forms of the species for this environment) also extending to near Roche lobe distances has also been of great importance, since these components can provide additional critical diagnostics of the upper atmosphere (Vidal-Madjar et al. 2004; Ben-Jaffel & Hosseini 2010). Their detection shows that heavy species are ef-

fectively entrained in the hydrodynamic outflow of the lighter hydrogen gas (through collisions with the neutral hydrogen atoms and the protons) and overcome diffusive separation (García Muñoz 2007; Koskinen et al. 2010, 2013a,b). The transit absorption depths in the O I 1304 Å and C II 1335 Å multiplets derived from the STIS G140L observations of HD 209458b were, respectively, $12.8 \pm 4.5\%$ and $7.5 \pm 3.5\%$ (Vidal-Madjar et al. 2004), or $10.5 \pm 4.4\%$ and $7.4 \pm 4.7\%$ from a re-visit of the observations (Ben-Jaffel & Hosseini 2010) and correspond to 2.8 and 2.2-sigma, or 2.4 and 1.6-sigma detections. These large absorption depths cannot be explained by 10,000 K thermal populations at solar abundances since line profiles that would result from thermal and natural broadening for vertical distributions from 1-D hydrodynamic models are not wide enough to significantly absorb the broad stellar lines (with solar line widths) during transit. This is explored in various papers (see below). Since the line absorption profiles and thus the velocity distributions of the absorbers were unresolved with STIS (using the G140L grating at $R \sim 1000$), substantially different interpretations have been put forth.

To broaden the absorption profile while keeping solar abundances, energetic super-thermal populations have been invoked (with effective temperatures $\times 5$ –100 larger than a $\sim 10,000$ K background H-dominated gas), such as from processes that preferentially energize minor species involving chemistry, radiation, and wave-particle interactions, or from turbulence and the stellar wind interaction (Ben-Jaffel & Hosseini 2010). Ben-Jaffel & Hosseini have shown that the final transit absorption profile is strongly dependent on the vertical distribution of the super-thermal population, a diagnostic that could be used if medium-resolution transit spectra are obtained. Alternatively, to enhance the optical thickness of the thermal population, some hydrodynamic models find that $\times 3$ –5 supersolar abundances would be required accompanied by a hotter thermosphere from twice the stellar XUV input than from the mean Sun (Koskinen et al. 2013b). (A previous hydrostatic approximation invoked quite large $\times 4$ –40 supersolar abundances with an unreasonably strong XUV flux $\times 5$ –10 higher than the mean Sun; Koskinen et al. 2010). However, recent findings are now showing an unexpected long-term low activity on the star HD 209458, and this low activity does not support scenarios that invoke even moderately high XUV fluxes, such as those of solar mean or maximum activity, to heat and inflate the atmosphere to the extent required by the observations (Ballester et al. 2015). As there appears to be an energy crisis in the upper atmosphere of this planet due to the low XUV input, new information on super-thermal processes that may operate in the upper atmosphere of this planet are needed, and such evidence is uniquely accessible with transit observations that resolve the line absorption profiles and thus velocity and energy distribution of the heavy species.

The Cosmic Origins Spectrograph (COS) on *HST* provides higher sensitivity than STIS, and it can improve the S/N of the transit absorption in C II 1335 Å and in O I 1304 Å as well as resolve the multiplets and the line absorption profiles at medium spectral resolution (with the G130M grating at $R \sim 20,000$) as has been demonstrated for the case of HD 189733b (Ben-Jaffel & Ballester 2013,

2014). FUV observations of the HD 209458 system were made with COS G130M by Linsky et al. (2010). Absorption by the planet during transit was reported in the C II 1335 Å doublet lines with a depth of $7.8 \pm 1.3\%$ in the -50 to $+50$ km s⁻¹ interval, similar to the line-integrated absorption detected with STIS. Tentative velocity signatures were reported, with absorption at -10 to 15 km s⁻¹ and less certain features at -40 and $+30$ – 70 km s⁻¹, and no absorption at zero velocity. The larger velocities would agree with the presence of an upper atmospheric hot population, or of plasma with large motions around the planet (Linsky et al. 2010; Koskinen et al. 2013b), with great implications about the properties of HD 209458b’s upper atmosphere.

From the same COS dataset, Linsky et al. (2010) also reported an $8.2 \pm 1.4\%$ transit absorption by Si III ions in the 1206.5 Å line. In sharp contrast, no Si III 1206.5 Å absorption was detected in the average of the four *HST* transit observations made with STIS G140L that detected O I and C II, where a negative result of $0.0_{-0.0}^{+2.2}\%$ was derived in Si III (Vidal-Madjar et al. 2004). To fit the COS Si III results, Koskinen et al. (2013b) found similar $\times 3$ – 5 supersolar abundances and higher stellar energy input requirements for the upper atmosphere, similar to the inferences made for the O I and C II.

The composition at high atmospheric altitudes (as modified by the stellar ionization, thermal balance, and charge-exchange processes) reflects the species and abundances at the base of the thermosphere, and it is thus diagnostic of the properties of the lower atmosphere and overall planetary abundances and energy budget (e.g., García Muñoz 2007; Koskinen et al. 2013a,b; Lavvas et al. 2014). This is particularly the case for a hot Jupiter with its strong 3D atmospheric circulation and large effective eddy mixing (e.g., Showman et al. 2009; Parmentier et al. 2013), and where the detection of extended O I and C II on HD 209458b itself shows that diffusive separation of the heavy species in the upper atmosphere is impeded by the hydrodynamic outflow (Koskinen et al. 2013a,b). For O I and C II the key lower atmospheric components are H₂O, that does not condense on hot Jupiters, and CO, the dominant carbon-bearing species on hot Jupiters (e.g., Moses et al. 2011). For refractory species like silicon, the situation is more complex and uncertain. For silicon to be present in the thermosphere, Koskinen et al. (2013b) find that it cannot condense into silicate clouds in the lower atmosphere, and that the vertical transport should be strong to keep any condensate particles lofted. Furthermore, silicon must be predominantly in the Si II ionization state, and charge exchange with protons (and He⁺) can then supply a significant Si III population to be detected. It may well be that silicon is not effectively removed by vertical and horizontal cold-traps on this planet, given the recent detection of Mg I in the upper atmosphere (Vidal-Madjar et al. 2013), but we must first address the validity of the reported COS detection of silicon ions, at least as Si III, given the contradiction with the negative STIS G140L results.

In this paper we re-visit the COS observations of the HD 209458 system given that these observations were not made in the standard fashion of observing immediately before and/or after the transit to contrast the in-transit

fluxes with the actual stellar fluxes around the time of transit. Instead, the in-transit stellar fluxes were ratioed against the average fluxes measured on three separate *HST* visits that were obtained over a period of one to two weeks with the planet off transit. The limitation of this approach is that the stellar activity, even if it is low, can cause significant flux variations in the FUV line emissions such as over a stellar rotation period, and from stochastic or flare activity (e.g., Parke Loyd & France 2014). This is indeed the case for the Sun for which a variation of $\sim 27\%$ was reported for the Si III 1206.5 Å line during a rotation period (e.g., Table 3 in Ben-Jaffel & Ballester 2013). It is thus possible that the transit absorptions derived from the COS data could be related to stellar variation rather than to the true planetary transit signature. Linsky et al. (2010) deduced their approach to be valid because the flux level and line shape in the Si IV 1393.7 Å line was similar in the in-transit data and in the averaged off-transit data. We find, however, that this use of the averaged off-transit data requires reassessment.

In Sec. 2 we re-evaluate the COS observations in the Si III 1206.5 Å line, C II 1335 Å doublet, Si IV 1393.7 Å line, and 1364.8–1390.7 and 1405.6–1423.6 Å continua, taking advantage of the temporal information of the data, both from the time-tagging and from comparison of the average stellar fluxes per *HST* visit. We find indeed significant time variation in the stellar emissions that render the previously derived transit absorptions for Si III 1206.5 Å line and the C II 1335 Å doublet from this COS dataset unreliable. Complications in the usage of the COS dataset for a derivation of velocity signatures in the absorption are also addressed. Moreover, we also present previously unpublished Si III transit observations of HD 209458b from a re-visit of the original STIS G140M dataset that discovered extended H I in Lyman- α absorption, since these exposures also sampled the Si III 1206.5 Å line. We find no evidence of a Si III transit absorption, in agreement with the first STIS G140L findings. We present and discuss the STIS data in Sec. 3. We also discuss some issues related to the conditions that would be needed in the lower atmosphere to obtain silicon ions in the upper atmosphere. We finish by establishing the need for COS FUV transit observations of this exoplanet, in particular for the unexploited diagnostics in the O I 1304 Å and C II 1335 Å transit signatures.

2. COS OBSERVATIONS

2.1. Observations and data reduction

HD 209458 was observed with COS on Sep–Oct 2009 during four *HST* visits, two or three *HST* orbits each, with the planet around orbital phases $\phi=0.27, 0.72, 0.0,$ and 0.49 (Table 1). The COS G130M grating was used covering the ~ 1130 – 1460 Å region at medium spectral resolution ($R \sim 20,000$ ~ 15 km/s, with 0.01 Å sampling). Throughout each visit the exposures were made alternating between four grating central wavelength settings referred to as 1291, 1300, 1309, and 1318. COS FUV spectra are sampled by two detector segments, A and B, that are separated by a small gap. Some of the grating settings either did not sample the important O I 1304 Å triplet or had the lines near the edge of the detector (Table 1), so this stellar emission could not be evaluated as was possible for transit observations of HD 189733b

TABLE 1
SUMMARY OF COS OBSERVATIONS

Exp. No.	Start time in 2009 (UT)	Exp. time (sec)	Planet mid. orbital phase	Grating wavelength setting ^a
01	Sep 19 10:10	2340	0.255	1291
02	Sep 19 11:36	0955	0.270	1300
03	Sep 19 11:55	1851	0.275	1309
04	Sep 19 13:11	0560	0.288	1300
05	Sep 19 13:24	2235	0.294	1318
06	Sep 24 13:12	2340	0.710	1291
07	Sep 24 14:38	0945	0.724	1300
08	Sep 24 14:57	1787	0.730	1309
09	Sep 24 16:14	0925	0.743	1300
10	Sep 24 16:33	1798	0.748	1319
11	Oct 02 14:32	1045	0.993	1291
12	Oct 02 14:53	1096	0.997	1300
13	Oct 02 15:55	1400	0.010	1309
14	Oct 02 16:22	1405	0.015	1319
15	Oct 18 10:51	1057	0.490	1291
16	Oct 18 11:18	1093	0.494	1300
17	Oct 18 12:20	1401	0.507	1309
18	Oct 18 12:46	1405	0.512	1319

^a The spectral ranges covered per grating wavelength setting respectively for detector Segments B & A are: (1291) 1132-1274 & 1291-1433 Å; (1300) 1141-1283 & 1300-1442 Å; (1309) 1153-1294 & 1309-1449 Å; and (1318) 1163-1303 & 1319-1459 Å.

(Ben-Jaffel & Ballester 2013, 2014). Note also that the C II 1335 Å feature is a triplet, but it is detected as a doublet with a line at 1334.5 Å and two unresolved lines at 1335.7 Å.

The time-tagged exposures were reprocessed into 100s segments, but since the S/N was low, the segments were averaged into 1000s sub-exposures so that the temporal flux variations (depicted in Fig. 1) were not dominated by the photon noise level. For the extraction of the stellar emission line fluxes, a weak stellar continuum was first subtracted from each spectrum based on a linear fit to the spectral regions devoid of obvious emission lines identified in a high-resolution solar spectrum (Curd et al. 2001). For the Si III 1206.5 Å line we also subtracted a linear fit of the blue wing of the stellar H I Lyman- α line which is very broad as detected by COS. This is a relatively small correction compared to the potential planetary absorption, and the associated errors have been included in the propagated errors. The stellar line fluxes, depicted in Fig. 1, were extracted by co-aligning the given line in all the spectra, and integrating the spectral fluxes out to about 10% of the averaged peak intensity (Ben-Jaffel 2007). This integration spanned about ± 28 km/s. Photon noise errors were propagated in all reduction steps and problematic pixels (with dq-wgt=0) were ignored.

2.2. Absolute Wavelength Scale

The determination of a common absolute wavelength scale, and thus of any planetary velocity signature reported from the COS dataset, was complicated because of having alternated between the four G130M central

wavelength settings during each visit. The original purpose of that setting was to minimize fixed-pattern noise and grid-wire shadow effects (France et al. 2010; Linsky et al. 2010), while for most other transit observations of exoplanets keeping instrumental settings fixed has proven best for measuring relative changes due to the planetary transmission alone. The grid-wire shadow effects are now automatically corrected by the COS pipeline software, as in the CALCOS 2.14.4 and 2.18.5 pipeline versions used for the time-tagged flux analysis and the wavelength study, respectively. The main complication is that the repositioning of the grating is not exactly repeatable due to thermal flexures (Shaw et al. 2009). Although in principle the absolute wavelength scale for each exposure could be set by co-aligning the C II 1334.5 Å line based on the dip from the ISM absorption of this line as done by Linsky et al. (2010), we found that the S/N is too low to accurately find the center of this absorption in each exposure. To co-align the spectra, for the Segment-A data we compared co-aligning the spectra against each line of the C II 1335 Å doublet and also against the full doublet. Significant differences were found when using only one line or the full doublet, when the data were smoothed or not, and when different exposures were chosen as the template. Comparing results from fitting against exposures 1 and 15 (Table 1), using only the C II 1334.5 Å line or the full doublet, and with or without smoothing, we found offsets in the centering of the ISM 1334.5 Å line absorption of about 10 km s^{-1} (about 5 pixels). This error, though somewhat smaller than the 15 km s^{-1} spectral resolution, produces large differences in the resulting line profiles and in the corresponding transit absorption line profile. In Fig. 2 (Sec. 2.4) we show a sample result of line profiles from co-alignment against exposure 15, using the full doublet, and with the data box-car smoothed by 5.

The Si III 1206.5 Å line data, sampled by the detector Segment B, was co-aligned separately. The wavelength shift found from the C II 1335 Å doublet in the Segment A data differed from that found for Segment B by up to ± 4 pixels (while Linsky et al. 2010 applied the same shift to data from both segments). This turned out to be expected since the COS pipeline calibration calculates the spectral offset for each detector segment independently. The SHIFT1A and SHIFT1B in the processed data differ by about 4–7 pixels, similar to the offsets that we found.

2.3. Time variation of the stellar fluxes

Figure 1 shows the time-resolved fluxes for the Si III 1206.5 Å line, C II 1335 Å doublet, Si IV 1393.7 Å line, and 1364.8–1390.7 and 1405.6–1423.6 Å continua. Black symbols show the fluxes from the 1000s sub-exposures, and gray symbols show the averaged fluxes per HST visit. For each feature, the fluxes have been normalized by the corresponding average value for visit 4 ($\phi \sim 0.49$) to ease the interpretation of the results. The error bars for the sub-exposures are propagated statistical photon noise, while the error bars for the visit-averaged fluxes include the non-statistical flux scattering within a given visit defined as the standard deviation from the mean. The variations within an HST visit can be stellar but there can also be instrumental effects (e.g., Linsky et al. 2012). Since the intra-orbit flux variations do not seem

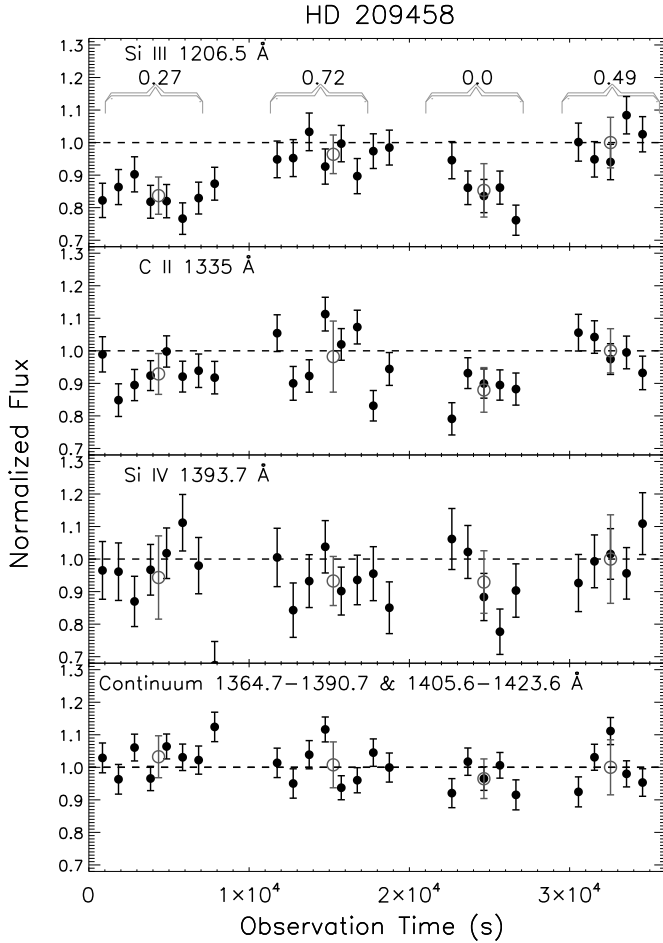


FIG. 1.— Normalized fluxes for the 1000s sub-exposures versus observation time for the stellar emission features Si III 1206.5 Å line, C II 1335 Å doublet, Si IV 1393.7 Å line, and the 1364.8–1390.7 & 1405.6–1423.6 Å continuum. The four HST visits are labeled on the top panel by the planetary orbital phase. For each visit the times have been offset from their arbitrary zero-time by 0 , 1×10^4 , 2×10^4 , and 3×10^4 s, respectively. For each emission feature, the average flux per visit is over-plotted as a gray circle at the middle of the visit.

repeatable from orbit to orbit, they cannot be systematically corrected for. The stellar fluxes averaged per visit are provided in Table 2 with both the photon-noise errors as well as errors that include the intra-visit scattering. In the discussion below we refer to the photon-noise errors for direct comparison with the results by Linsky et al. (2010).

To evaluate the validity of deriving a transit absorption from this COS dataset we look at the normalized fluxes averaged per HST visit (Table 2). For the C II 1335 Å doublet we find that although the flux during transit ($\phi = 0.0$) is low at 0.880 ± 0.021 , the flux is also relatively low for $\phi = 0.27$ at 0.929 ± 0.017 . In contrast, the flux for $\phi = 0.72$ of 0.982 ± 0.018 is similar to the reference value of 1.0 ± 0.023 for $\phi = 0.49$ within the errors. Although the transit depth relative to the mean of the off-transit fluxes (at $\phi = 0.27$, 0.72 , and 0.49) would be $9.3 \pm 2.4\%$, which is somewhat deeper than the $7.8 \pm 1.3\%$ reported by Linsky et al. (2010), the range of depths rela-

TABLE 2
NORMALIZED STELLAR FLUXES FROM COS DATASET, AVERAGED PER HST VISIT

Spectral feature	Planet mid. orb. phase	Norm. flux ^a	Photon noise error	Intra-visit std error ^b	Photon and intra-visit error ^b
Si III 1206.5 Å line	$\phi = 0.27$	0.837	0.018	0.054	0.057
	$\phi = 0.72$	0.964	0.020	0.056	0.059
	$\phi = 0.00$	0.853	0.023	0.079	0.082
	$\phi = 0.49$	1.000	0.025	0.074	0.078
C II 1335 Å doublet	$\phi = 0.27$	0.929	0.017	0.060	0.063
	$\phi = 0.72$	0.982	0.018	0.108	0.109
	$\phi = 0.00$	0.880	0.021	0.065	0.069
	$\phi = 0.49$	1.000	0.023	0.064	0.068
Si IV 1393.7 Å line	$\phi = 0.27$	0.943	0.029	0.125	0.128
	$\phi = 0.72$	0.933	0.029	0.070	0.075
	$\phi = 0.00$	0.929	0.036	0.089	0.096
	$\phi = 0.49$	1.000	0.038	0.131	0.136
1364.8–1390.7 & 1405.6–1423.6 Å continuum	$\phi = 0.27$	1.032	0.015	0.063	0.064
	$\phi = 0.72$	1.008	0.015	0.069	0.070
	$\phi = 0.00$	0.965	0.019	0.058	0.061
	$\phi = 0.49$	1.000	0.019	0.083	0.085

^a The fluxes have been normalized with respect to the average of visit 4 ($\phi = 0.49$), given by: 2.12×10^{-15} for Si III; 2.33×10^{-15} for C II; 0.96×10^{-15} for Si IV, and; 4.87×10^{-15} ergs cm⁻² s⁻¹ for the continuum.

^b The intra-visit error is the standard deviation of the scattering of the stellar flux during the given visit.

tive to the different average fluxes for the off-transit visits spans from $5.3 \pm 2.9\%$ to $12.0 \pm 2.9\%$. The detection and depth of the C II 1335 Å transit signature of HD 209458b associated thus far with the COS instrument remains unconfirmed given the inappropriate observing method that was employed.

The Si III 1206.5 Å line also shows a strong time variation. A low flux of 0.837 ± 0.018 is observed at $\phi = 0.27$ and a similar value of 0.853 ± 0.023 is seen during transit. Furthermore, the flux of 0.964 ± 0.020 observed at $\phi = 0.72$ is comparable to the reference value of 1.0 ± 0.025 at $\phi = 0.49$ within the errors. Deriving a transit absorption for Si III is therefore misleading, given the large time variations. A detection of Si⁺⁺ ions in the upper atmosphere of HD 209458b is not valid from this COS dataset.

The 1364.8–1390.7 & 1405.6–1423.6 Å continuum consists of the photospheric continuum (that decreases towards shorter wavelengths) and a white continuum emission from the chromosphere (that increases towards shorter wavelengths; Linsky et al. 2012). No large continuum-flux variations are observed in tandem with the line emissions, indicating that no large common-mode instrumental effect was at play. This chromospheric component is expected to vary with stellar activity, yet the variability at these wavelengths should be smaller than in any of the emission lines (e.g., Snow et al. 2010). Although in the observation at $\phi = 0.27$ the continuum did not appear relatively low as in the other features but was instead somewhat larger, and during the transit visit it was relatively low as could be due to the transit of the planetary disk, the fluxes are all similar within the errors.

For the Si IV 1393.7 Å line (significantly brighter than

TABLE 3
 HD 209458 AVERAGE STELLAR FLUXES FROM COS DATASET, AND
 APPARENT VISIT-TO-VISIT VARIATIONS FROM OFF-TRANSIT DATA

Spectral feature	Flux ^{a,b}	%Variation ^b	%Variation ^b
	(10 ⁻¹⁵ ergs/cm ² /s)	as a std. dev.	as a max/min
Si III 1206.5 Å line	1.98±0.15	7.5%	19.4±8.3%
C II 1335 Å doublet	2.26±0.07	3.1%	7.7±5.4%
Si IV 1393.7 Å line	1.47±0.05	3.1%	7.2±10.7%
1364.8–1390.7 & 1405.6–1432.6 Å cont.	4.94±0.07	1.4%	3.2±5.0%

^a Mean spectral flux and standard deviation.

^b Errors include intra-visit noise.

the other 1402.8 Å line of the doublet), we find that the fluxes are relatively low not only at both $\phi = 0.0$ and 0.27, but also at $\phi = 0.72$ unlike for Si III and C II for which the fluxes at $\phi = 0.72$ were higher and comparable to the fluxes at $\phi = 0.49$. Thus, the stellar Si IV emission turns out not to be an accurate proxy for the C II and Si III emissions.

The variations of the emissions as observed in the off-transit visits are listed in Table 3. Clearly, the 7.5% variation (or 19.4±8.3% max/min) of the Si III 1206.5 Å flux is quite large, more so than for the C II 1335 Å or Si IV 1393.7 Å fluxes although there may be some overlap if the intra-visit scatter is included in the errors.

It is interesting to note that the 3.1% variation (or 7.2±10.7% max/min) of the Si IV 1393.7 Å line is smaller than the 7.5% variation of the Si III 1206.5 Å line (or 19.4±8.3% max/min) for the same set of observations (although again they overlap within the larger error bars). Since the Si IV 1393.7 Å emission originates from a hotter layer in the stellar atmosphere (at $\log T = 4.75$ for the Sun) than the C II 1335 Å and Si III 1206.5 Å emissions (at $\log T = 4.10$ and 4.25, respectively; Woods et al. 2000) it would be expected in general to vary more strongly or at least comparably to the Si III 1206.5 Å line (based on more variability at higher temperature regions).

Solar observations indicate that the Si IV 1398 Å doublet variability is comparable in general to that of the Si III 1206.5 Å line, or somewhat larger at high activity as known from short-term and long-term observations and from observations of flares (Woods et al. 2000; Brekke et al. 1996). However, a recent evaluation of the solar variability in the FUV emission lines relevant to hot-Jupiter transit studies has been made by Ben-Jaffel & Ballester (2013) using 2003–2007 spectra from the Solar Stellar Irradiance Experiment (SOLSTICE) instrument on-board the *Solar Radiation and Climate Experiment (SORCE)* obtaining more detailed or relevant results for exoplanet FUV *HST* work. The data were divided into periods of low, medium, high, and extreme flare activity, where the lower activity should include the emission from plages and enhanced network. In three out of four flare level categories, the variability of the Si IV 1398 Å doublet is comparable to that of the Si III 1206.5 Å line, and somewhat larger for the cases of high activity in agreement with the findings by Woods et al. (2000). In that study, there was a sepa-

rate evaluation for the Si IV 1393.7 Å line (see bottom part of Table 3 in Ben-Jaffel & Ballester 2013). The solar Si IV 1393.7 Å line showed, in contrast, that the variability with solar 27-day rotation and 11-year cycle was somewhat smaller, at 22 and 60%, respectively, compared to 27 and 73% for the Si III 1206.5 Å line. (These variabilities are also standard deviations from the mean.) The solar lines do show more variability than the COS results for HD 209458, but the COS dataset is extremely limited to three samples. Here we present results for the Si IV 1393.7 Å line and not the doublet, since this was the line used by Linsky et al. (2010) as a proxy for the stellar activity given that it is about twice as bright as the second line in the doublet. In a separate analysis of the COS dataset (not presented here) in which we have not divided the exposures into time-tagged segments, we see that the variation in the full doublet is larger and more comparable to that of the Si III 1206.5 Å line, due to inclusion of the more variable and/or noisier second line in the doublet. Parke Loyd & France (2014) report on temporal variations on FUV fluxes of sunlike stars in 60-second time intervals. For HD 209458 they report upper limits for the variation in the Si III 1206.5 Å line and Si IV 1398 Å doublet emissions (which is not surprising given the relatively low S/N of the data), and their upper limit variation for the Si IV doublet is a bit larger than for the Si III line. Therefore, from the various lines of evidence presented, it is unclear at this point if the relatively low visit-to-visit variation of the Si IV 1393.7 Å line compared to the larger variation in the Si III 1206.5 Å line is significant and distinct for this star compared to the Sun. The degree of intra-visit scatter for both features seems comparable, however, although the COS data is extremely limited. Future observations should shed more light into the simultaneous temporal FUV flux variations on this star.

Finally, it is also interesting that the Si III 1206.5 Å and C II 1335 Å emissions may have shown a stellar rotational variation. Visits 1, 2, 3, and 4 were made on days 0 (reference date), 5, 13, and 29. Using the stellar rotation periods of $\sim 11.2 - 14.1$ days derived from the Rossiter-McLaughlin effect and the stellar line widths provided in the literature (c.f., Ballester et al. 2015), these visits corresponded to stellar rotational phases of 0 (reference phase), 131–165, 336–63, and 20–212°. Therefore, visits 1 and 3 that showed the lowest fluxes should correspond to similar stellar phases, around the reference phase 0°.

We emphasize, however, that the COS dataset at hand is extremely limited, consisting of only a single in-transit observation visit and three off-transit visits on separate dates. To definitely ascribe a stellar rotational modulation to the Si III 1206.5 Å and C II 1335 Å stellar fluxes would be premature, since there can be stochastic effects. Furthermore, to derive a reliable transit absorption based on the observing technique used for the COS dataset, one would have to observe many times with the planet both in-transit and off-transit, to hopefully average-out potential rotational, stochastic, small flaring activity, and long-timescale magnetic cycle variations in the stellar fluxes. Such extensive observations are not viable with *HST*. Instead, the standard transit method of directly measuring the actual stellar flux immediately before and/or after transit is by far the most direct and

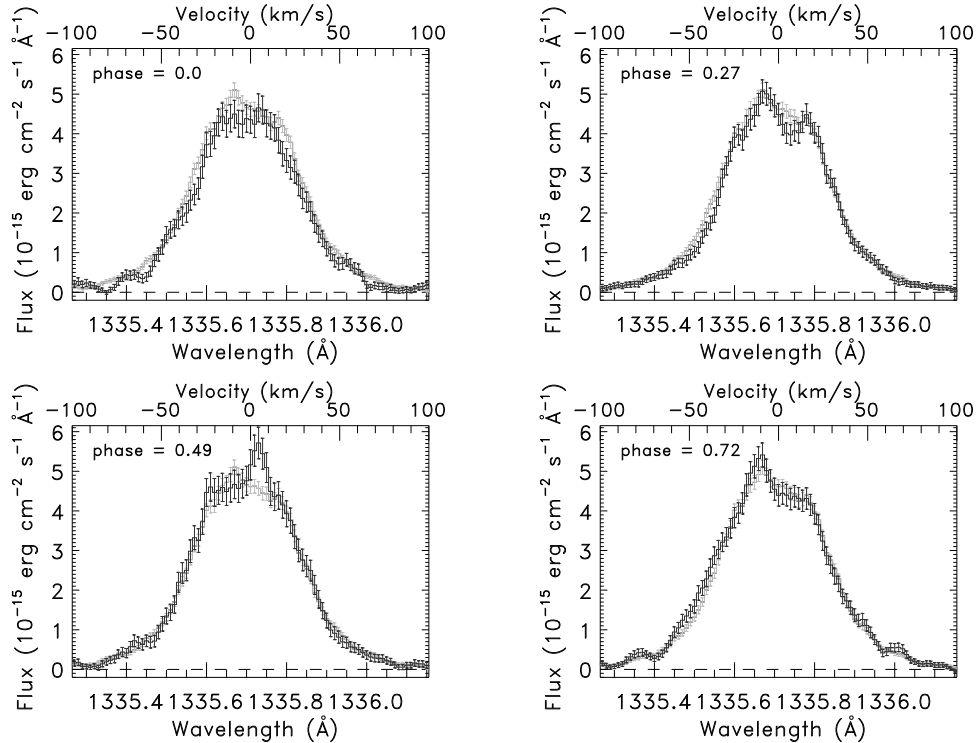


FIG. 2.— Sample shapes of the C II 1335.7 Å line derived from the COS data of the four *HST* visits, box-car smoothed by 5, with error bars. The gray profile is the average off-transit data ($\phi = 0.27, 0.49, 0.72$). To correct for non-repeatable wavelength offsets from alternating the grating setting, the data were co-aligned against exposure #15, using both lines of the C II 1335 Å doublet. Visit-to-visit variation in the stellar line shape is apparent, but observations with a single grating setting should be more suitable to determine the stellar behavior.

least ambiguous FUV transit observational method, as well as the one that would utilize the least *HST* resources. Already, the time variation found in the stellar fluxes in this COS dataset clearly demonstrates this argument.

2.4. Problems with the reported velocity distribution of the absorbers

COS G130M transit observations of HD 209458b have high enough sensitivity and spectral resolution to potentially determine the velocity distribution of the absorption by the heavy species on the planet at similar S/N as in the STIS G140M observations of the H I Lyman- α line absorption (Vidal-Madjar et al. 2003, 2008; Ben-Jaffel 2007, 2008; Ben-Jaffel & Hosseini 2010). This has been demonstrated for both the C II 1335 Å doublet as well as the O 1304 Å triplet transit observations of HD 189733b (Ben-Jaffel & Ballester 2013). Figure 2 shows the average C II 1335.7 Å line profiles for the four *HST*/COS visits of HD 209458. Although there may be real planetary atmospheric absorption during transit ($\phi = 0$), we find an apparent visit-to-visit variation in the average off-transit stellar line shapes that precludes a proper evaluation of the velocity signature in the planetary absorption. For these reasons of potential intrinsic time variation in the stellar line shapes, the velocity distribution of the absorbers reported by Linsky et al. (2010) for HD 209458b from the COS dataset at hand is invalid. We note that the apparent stellar line-shape variation may be related instead to errors in the co-alignment of the spectra that was needed since the multiple grating wavelength settings were not exactly repeatable as described in Sec. 2.2, but this cannot be fully explored with this dataset.

TABLE 4
SUMMARY OF STIS G140M OBSERVATIONS

Exp. No.	Start time in 2001 (UT)	Exp. time (sec)	Planet mid. orbital phase
o6e201010	Sep 07 20:35	1780	0.980
o6e201020	Sep 07 22:13	2100	0.000
o6e201030	Sep 07 23:49	2100	0.019
o6e202010	Sep 14 21:12	1780	0.973
o6e202020	Sep 14 22:42	2100	0.992
o6e202030	Sep 15 00:18	2100	0.011
o6e203010	Oct 20 02:50	1780	0.969
o6e203020	Oct 20 04:20	2100	0.988
o6e203030	Oct 20 05:56	2100	0.007

Proper COS transit observations are needed, with consecutive data with the planet in and out of transit, and using a single grating wavelength setting (Sec. 2.2).

3. STIS G140M AND G140L OBSERVATIONS: NO Si III DETECTION

The *HST* STIS medium-resolution G140M transit observations that discovered the extended hydrogen atmosphere on HD 209458b (Vidal-Madjar et al. 2003; Ben-Jaffel 2007) also sampled the Si III 1206.5 Å line. With a resolving power of $R \sim 10,000$, the line is spectrally resolved and well separated from the wings of the Lyman- α line although the S/N is relatively low. Three transit observations were made (Table 4). Figure 3 shows the line fluxes per *HST* visit, integrated at 1206.5.07–1207.14 Å and normalized to the average of the first two

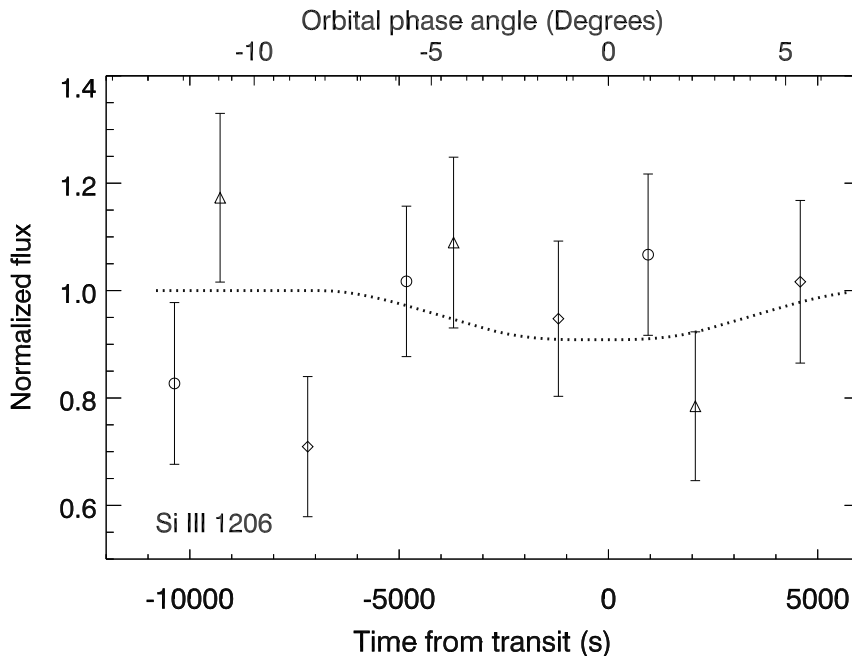


FIG. 3.— Stellar fluxes in the Si III 1206.5 Å line for three transits of HD 209458b observed with STIS G140M, the same dataset that discovered an extended H I atmosphere on this planet (Vidal-Madjar et al. 2003; Ben-Jaffel 2007). Diamonds for 7–8 Sep. 2001; triangles for 14–15 Sep. 2001; and circles for 20 Oct. 2001. The fluxes are normalized to the 1.56×10^{-15} ergs cm $^{-2}$ s $^{-1}$ average of the first two points. The data are integrated per *HST* orbit (3 orbits per transit). The transit light curve is drawn for an atmosphere obscuring 8.9% of the star (Ben-Jaffel 2007).

points of 1.56×10^{-15} ergs cm $^{-2}$ s $^{-1}$. No Si III transit absorption is detected. The ratio of the average of the three points within 3000s from mid-transit to the first three off-transit points yields a negative result of $1.7 \pm 18.7\%$ absorption. The 1.7% absorption, if real, would represent the 1.5% obscuration by the disk of the planet.

Although the S/N is low, large temporal variations are clearly present, from visit to visit, and intra-visit. The std. dev. is 13% for the off-transit points, and 15% for all the data. Thus, as with the COS observations discussed in Sec. 2.3, we find significant variation in the stellar Si III emission. The 13% std. dev. variation of the off-transit data found with STIS is about twice the 7.5% value found with COS.

The original STIS G140L observations sampled four partial transits and a negative detection in Si III 1206.5 Å was reported with a transit absorption of $0.0_{-0.0}^{+2.2}\%$ by Vidal-Madjar et al. (2004). The non-detection was later confirmed by Ben-Jaffel & Hosseini (2010). Although a limitation of the low-resolution G140L data is the contamination of the Si III line by the blue wing of the stellar Lyman- α line, and the S/N in the (lower sensitivity) G140M data is low, taken together, there are now seven transits observed with STIS that do not show Si III absorption.

A summary of the current transit results of heavy species on HD 209458b with STIS and COS is provided in Table 5, including the new results from STIS. We also include transit depths from Linsky et al. (2010) from the 2009 COS dataset and those discussed in Sec. 2 for comparison, although all of these depths are not valid since

the stellar flux around the time of transit is unknown. For valid COS results new observations are required sampling the transit light curve.

4. DISCUSSION: NEW LIGHT ON CONTRIBUTION OF UV STUDIES TO EXOPLANETARY ATMOSPHERIC SCIENCES

The abundance of heavy species in the upper atmosphere has major implications on all pressure levels from the top to the bottom of a planetary atmosphere. The link of the FUV transit observations with properties of the planet and its lower atmosphere are often underplayed. The mere detection of extended O I and C II absorption in HD 209458b’s upper atmosphere with STIS G140L (at low spectral resolution) already requires solar or supersolar abundances, a firm result that is in sharp disagreement with the recent inference of potential $\times 20$ – 125 low metallicity on this planet (Madhusudhan et al. 2014). This low metallicity has been raised as one of two explanations for an inferred low H $_2$ O abundance in the planet’s lower atmosphere: either a low metallicity and C/O < 1 since water would be the major oxygen-bearing species in this case, or; a high metallicity but C/O > 1. A $\times 20$ – 125 low metallicity would be highly unexpected on a hot Jupiter. (Note that HD 209458 has a solar metallicity [Fe/H]= -0.0 ± 0.2 ; Mazeh et al. 2000.) The goal of Madhusudhan et al. (2014) is to explain a low contrast $1.4 \mu\text{m}$ band absorption reported for this planet from *HST* Wide-Field Camera 3 transit data, yet, it is possible that some level of haze scattering is present (Deming et al. 2013), as well as that the data need further work (T. Evans et al., in progress). Since species in

TABLE 5
CURRENT TRANSIT RESULTS FOR HEAVY SPECIES IN THE UPPER ATMOSPHERE OF HD 209458B

Instrument mode	Species feature (Å)	Species feature (Å)	Species feature (Å)	Species feature (Å)	Ref.
<i>Absorption depths from transit light curve FUV observations</i>					
	O I 1304 triplet	C II 1335 doublet	Si III 1206.5 line	Si IV 1393.7 line	
STIS G140L	12.8±4.5%	7.5±3.5%	0.0 ^{+2.2%} _{-0.0%}	0.0 ^{+6.5%} _{-0.0%}	Vidal-Madjar et al. (2004) ^a
STIS G140L	10.5±4.4%	7.4±4.7%	confirmed	confirmed	Ben-Jaffel & Hosseini (2010) ^a
STIS G140M	n/a	n/a	1.7±18.7%	n/a	this work ^a
<i>Invalid depth estimates from COS 2009 dataset from in-transit data against data from other dates</i>					
		C II 1335 doublet	Si III 1206.5 line	Si IV 1393.7 line	
COS G130M		7.8±1.3%	8.2±1.4%	0.00±0.01%	Linsky et al. (2010) ^b
" , this work		9.3±2.4%	8.6±2.7%	3.1±4.2%	vs off-tr. ave, photon noise ^c
" , this work		5.3±2.9%	-1.9±3.5%	1.5±4.9%	vs $\phi = 0.27$, photon noise ^d
" , this work		9.3±8.4%	8.6±9.5%	3.1±12.1%	vs off-tr. ave, w intra-visit var. ^e
" , this work		5.3±9.8%	-1.9±12.0%	1.5±16.8%	vs $\phi = 0.27$, w intra-visit var. ^e

^a The STIS G140L and G140M results were respectively derived from 4 and 3 transit observations.

^b Invalid "transit depth" reported by Linsky et al. (2010), not from a transit light curve but from the average of data with the planet off-transit at orbital phases $\phi = 0.27, 0.72$ and 0.49 , and with errors for photon noise only.

^c As in item *b*, for comparison with the Linsky et al. results, with photon noise only.

^d Sample invalid "transit depth" from contrasting the in-transit data against off-transit observation at $\phi = 0.27$. A negative detection is obtained in Si III, and a smaller transit depth is obtained in C II.

^e Invalid "transit depths" derived as in items *c* or *d* but including the intra-visit standard-deviation variations (Table 2) in the errors. No previous HD 209458b UV transit study has included this variation. Full transit light curves are needed for a proper assessment of these variations and thus of the true potential of the COS transit measurements of HD 209458b.

the upper atmosphere derive from dissociation products in the lower atmosphere, issues of metallicity and C/O ratio are directly testable with FUV observations – provided high quality data resolving the transit absorption line shapes are obtained.

The presence of Si III in the upper atmosphere of HD 209458b would have implied that silicon gas is not effectively depleted by cloud condensation in the lower atmosphere (Koskinen et al. 2013a,b; Lavvas et al. 2014). This turns out to possibly still be the case as demonstrated by the recent detection of $6.2 \pm 2.9\%$ absorption (or $8.8 \pm 2.1\%$ if there was still post-egress absorption) by extended Mg I on this planet at near-solar abundance (Vidal-Madjar et al. 2003), because magnesium and silicon condense together into silicate grains of fosterite and enstatite (Visscher, Lodders & Fegley 2010). The detection of magnesium in the thermosphere of HD 209458b indicates that the balance of day-to-night temperature (Showman et al. 2009; Moses et al. 2011; Crossfield et al. 2012) against the strong vertical and horizontal 3D dynamics (Showman et al. 2009; Spiegel et al. 2009; Parmentier et al. 2013) impedes significant condensation and settling of refractory silicate species on this planet (Koskinen et al. 2013a,b; Lavvas et al. 2014). If condensation takes place, such as on the nightside, the transport of fine silicate grains onto hotter high-altitude dayside regions may allow for effective sublimation on this hot Jupiter. Such a strong transport of fine grains has been found to be possible on HD 209458b based on 3D global circulation modeling that included test particles and found a strong circulation with large effective eddy coefficients of for example $K_{zz} \sim 10^{10} \text{ cm}^2 \text{ s}^{-1}$ at $P \sim 1 \text{ mbar}$ (Parmentier et al. 2013).

With respect to the FUV and NUV observations and the upper-atmosphere modeling, the disagreement lies in

the predicted Si III and observed Mg I ionization states, such that silicon might be present mainly as either Si I or Si II. In the latter case charge-exchange reaction rates invoked to convert part of the Si II into Si III would need to have been overestimated so that no significant Si III 1206.5 Å absorption is detected in transit. The charge exchange of Si II with protons ($\text{Si}^+ + \text{p}^+ \rightarrow \text{Si}^{++} + \text{H}$) was first proposed by Linsky et al. (2010) as the main source of Si III since this reaction has been found to be relevant for the Sun. In their detailed upper-atmosphere models for HD 209458b that included heavy metal species, Koskinen et al. (2013a,b) confirmed that this reaction is key in producing detectable amounts of Si III to fit the $\sim 8\%$ transit depths reported by Linsky et al. from the COS dataset. However, our new STIS G140M negative finding for Si III on this planet that is consistent with the previous negative detection by Vidal-Madjar et al. (2004) (Table 5), poses new questions into the modeling and/or the state of the upper atmosphere of this planet. It may be that the model temperatures are too high since temperatures above $\sim 15,000 \text{ K}$ are required for the Sun to produce significant Si III abundances (Baliunas & Butler 1980) and these temperatures do not necessarily apply to this planet. The model temperature depends on the chemical composition, on the stellar XUV input and the heating efficiency, and on the velocity of the outflow since it can adiabatically cool the atmosphere, although there are always uncertainties in these calculations. We find in the literature that only models with high stellar XUV input and high heating efficiency seem to reach high temperatures of $15,000 \text{ K}$ and beyond, such as all the model cases in Tian et al. (2005), the subsonic cases in García Muñoz (2007), and the models in Koskinen et al. (2013a,b) that explicitly assume a $\times 10$ or $\times 100$ higher solar XUV input for the star. Other

models reach about 12,000–14,000 K peak temperatures, such as the Yelle (2004) model, the super-sonic cases in García Muñoz (2007), and the Koskinen et al. (2013a,b) models with solar XUV input. In the modeling of the upper atmosphere of a non-magnetized HD 209458b and its interaction with the stellar wind, Murray-Clay et al. (2009) find that the peak temperature reaches $\sim 10,000$ K for a solar XUV flux, while for a 1000 times larger XUV flux typical of young T-Tauri stars the peak temperature reaches only slightly larger values due to radiative HI Lyman- α cooling rather than by the expansion of the gas. In a separate work we are finding evidence that the star HD 209458 has a surprising long-term low activity, and this indicates that the star provides a significantly lower XUV input to the planet than assumed in all previous modeling (Ballester et al. 2015). In that work we apply the detailed photochemical hot-Jupiter upper-atmosphere models of García Muñoz (2007) that include detailed photochemistry for both ion and neutral species of H, D, He, O, C and N and for which we have updated our best current estimate of the stellar X-ray and UV input. The modeling finds indeed peak atmospheric temperatures (for solar abundances) of only $\sim 10,000$ K. Given the Mg I detection, and accompanying non-detection of Mg II (Vidal-Madjar et al. 2013), the dominant silicon ionization state may be Si I since Mg I and Si I have similar ionization potentials. Nevertheless, the finding that Mg I dominates in the upper atmosphere of this planet is highly unexpected, since significant photoionization ($\lambda < 1621 \text{ \AA}$) should be present while Mg II was not positively detected. This seems to require very large electron densities for the dielectric recombination required to counteract photo-ionization: for example, at the reference altitude of $r = 3R_p$ Bourrier et al. (2014) require at least two orders of magnitude higher electron densities than estimated from current hydrodynamic models (García Muñoz 2007; Koskinen et al. 2013a,b; Guo 2013; Lavvas et al. 2014; Ballester et al. 2015). This is something that is rather hard to explain.

Another finding is that the Mg I 2853.0 \AA line absorption seems to be blue-shifted to -62 to -19 km s^{-1} (Vidal-Madjar et al. 2013). This finding is quite compelling to some and unexpected to others, as per the discussion in the Introduction related to the HI Lyman- α line. Again, the large electron densities required for dielectronic recombination and the fast outflows needed at the exobase to explain the Mg I blue-shifted absorption by stellar radiation pressure (Bourrier et al. 2014) are difficult to reconcile with current upper atmosphere models. Yet, if confirmed, the Mg I blue-shifted absorption reveals a net anti-solar motion that may apply to one or more components of the upper atmosphere. Do the O I and C II species also show a net blue-shifted absorption? Are the motions of the ions and neutrals fully coupled (e.g., García Muñoz 2007; Trammell et al. 2011; Adams 2011) or are they decoupled at large enough distances and low collision rates (e.g., Koskinen et al. 2014)? The latter could be expected from effects by different radiation pressure, charge exchange with the stellar wind protons, close and open planetary magnetic-field lines and decaying field strength with distance, and net magnetospheric currents and convection. Velocity-resolved transit data on the C II 1335 and O I 1304 \AA lines, even

if only separating the blue- and red-component absorptions, would provide much needed tools for characterizing the state of the upper atmosphere of HD 209458b that is still an enigma. Such data can be obtained with COS.

5. CONCLUSIONS

We have presented new STIS G140M transit data reinforces the original results with STIS G140L that Si III ions are not detected in the thermosphere of HD 209458b. Silicon may still be present in the upper atmosphere, but at a lower ionization state that may even be Si I, based on the independent *HST* detection of extended Mg I on this planet which also indicates that silicate condensation and cold trapping is not 100% effective in the lower atmosphere. The models for HD 209458b by Koskinen et al. (2013a,b) that include refractory species already predict Si II to be dominant silicon species in the upper atmosphere, so what is needed as a first step is to limit the yield for Si III. A second step much harder to address would be whether the silicon is in the Si II or Si I state, given the positive Mg I but negative Mg II detection on HD 209458b by Vidal-Madjar et al. (2013) and that Si I and Mg I have similar ionization potentials. The lack of a positive Si III detection in the extended atmosphere of the planet reported in this work, together with the positive Mg I detection and the long-term low activity now being identified for the star Ballester et al. (2015) indicate that a revision to our present understanding of the upper atmosphere of this planet is needed. Much new insight can be obtained with new COS FUV transit observations.

The existing COS G130M observations of the HD 209458 system were not standard transit observations and significant stellar flux variations found in the data invalidate previously reported transit results. Proper FUV transit observations with COS are needed, sampling the transit light curve (at a single grating wavelength setting). These observations will independently confirm and measure transit depths in the O I and C II species at high S/N, and furthermore resolve the velocity distribution of the O I and C II species with major implications on upper atmospheric dynamics, energetics and magnetospheric processes, as well as on the species abundances that are also relevant for the characterization of the planet and its lower atmosphere. In this frame, the detection of O I and C II in the upper atmosphere of HD 209458b using only unresolved lines already requires solar or supersolar abundances that are in disagreement with a very low metallicity as recently considered in the literature. In the near future, upper atmospheric UV studies of exoplanets may prove key for unraveling the so far elusive properties of low mass exoplanets.

We are grateful to Brian York and Justin Ely at the HST Help Desk for input on COS observations and data re-processing. We thank F. Pont, D. Sing, P. Lavvas, A. García Muñoz, A. Showman, V. Parmentier, and T. Koskinen for interesting conversations on metallicity, condensation, circulation, and upper atmospheres of hot Jupiters applicable to this work. We also thank the referee for helpful suggestions on the manuscript. LBJ acknowledges support from CNES, Université Pierre et Marie Curie and the Centre National de la Recherche

Scientifique in France. He also acknowledges his current appointment as a Visiting Research Scientist at the Dept. of Planetary Sciences and the Lunar and Planetary Laboratory of the University of Arizona. GEB was partially

funded by the Space Telescope Science Institute under grants HST-GO-12473.01-A and HST-AR-11303.01-A to the University of Arizona.

Facilities: HST (STIS), HST (COS).

REFERENCES

- Adams, F. C. 2011, *ApJ*, 730, 27
 Baliunas, S. L. & Butler, S. E. 1980, *ApJ*, 235, L45
 Ballester, G. E., Ben-Jaffel, L., García Muñoz, A., Sanz-Forcada, J., Henry, G. W., & Sing, D. K. 2015, *ApJ*, in prep.
 Ben-Jaffel, L. 2007, *ApJ*, 671, L61
 Ben-Jaffel, L. 2008, *ApJ*, 688, 1352
 Ben-Jaffel, L. & Hosseini, S. S. 2010, *ApJ*, 709, 1284
 Ben-Jaffel, L. & Ballester, G. E. 2013, *A&A*, 553, A52
 Ben-Jaffel, L. & Ballester, G. E. 2014, *ApJ*, 785, L30
 Brekke, P., Rottman, G. J., Fontenla, J., & P. G. Judge 1996, *ApJ*, 468, 418
 Bourrier, V., Lecavelier des Etangs, A., Dupuy, H., et al. 2013, *A&A*, 551, A63
 Bourrier, V. & Lecavelier des Etangs, A. 2013, *A&A*, 557, A124
 Bourrier, V., Lecavelier des Etangs, A., & Vidal-Madjar, A. 2014, *A&A*, 565, A105
 Cohen, O. & Glöcer, A. 2012, *ApJ*, 753, L4
 Crossfield, I. J. M., Knutson, H., Fortney, J., et al. 2012, *ApJ*, 752, 81
 Curdt, W., Brekke, P., Feldman, U., et al. 2001, *A&A*, 375, 591
 Deming, D., Wilkins, A., McCullough, P., et al. 2013, *ApJ*, 774, 95
 France, K., Stocke, J. T., Yang, H., et al. 2010, *ApJ*, 712, 1277
 García Muñoz, A. 2007, *Planet. Sp. Sci.*, 55, 1426
 Guo, J. H. 2011, *ApJ*, 733, 98
 Guo, J. H. 2013, *ApJ*, 766, 102
 Holmström, M., Ekenbäck, A., Selsis, F., et al. 2008, *Nature*, 451, 970
 Khodachenko, M. L., Alexeev, I., Belenkaya, E., et al. 2012, *ApJ*, 744, 70
 Kislyakova, K., Holmström, M., Lammers, H., Odert, P. & Khodachenko, M. L. 2014, *Science*, 346, 981
 Koskinen, T. T., Yelle, R. V., Lavvas, P., & Lewis, N. K. 2010, *ApJ*, 723, 116
 Koskinen, T. T., Harris, M. J., Yelle, R. V., & Lavvas, P. 2013a, *Icarus*, 226, 1678
 Koskinen, T. T., Yelle, R. V., Harris, M. J., & Lavvas, P. 2013b, *Icarus*, 226, 1695
 Koskinen, T. T., Yelle, R. V., Lavvas, P., & Cho, J. Y.-K. 2014, *ApJ*, 796, 16
 Kulow, J. R., France, K., Linsky, J., & Parke Loyd, R. O. 2014, *ApJ*, 786, 132
 Lammer, H., Selsis, F., Ribas, I., et al. 2003, *ApJ*, 598, L121
 Lavvas, P., Koskinen, T., & Yelle, R. V. 2014, *ApJ*, 796, 15
 Lecavelier des Etangs, A. 2007, *A&A*, 461, 1185
 Lecavelier des Etangs, A., Vidal-Madjar, A., Hébrard, G., & McConnell, J. 2004, *A&A Letters*, 418, L1
 Lecavelier des Etangs, A., Bourrier, V., Wheatley, P. J., et al. 2012, *A&A Letters*, 543, L4
 Linsky, J. L., Yang, H., France, K., et al. 2010, *ApJ*, 717, 1291
 Linsky, J. L., Bushinsky, R., Ayres, T., Fontenla, J., & France, K. 2012, *ApJ*, 745, 25
 Madhusudhan, N., Crouzet, N., McCullough, P. R., Deming, D., & Hedges, C. 2014, *ApJ*, 791, L9
 Moses, J. I., Visscher, C., Fortney, J. J., et al. 2011, *ApJ*, 737, 15
 Mazeh, T., Dominique, N., Torres, G., et al. 2000, *ApJ*, 532, L55
 Murray-Clay, R. A., Chiang, E. I., & Murray, N. 2009, *ApJ*, 693, 23
 Owen, J. E. & Adams, F. C. 2014, *MNRAS*, 444, 3761
 Parmentier, V., Showman, A. P., & Lian, Y. 2013, *A&A*, 558, A91
 Parke Loyd, R. O. & France, K. 2014, *ApJS*, 211, 9
 Shaw, B., Massa, D., Kaiser, M. E., et al. 2009, *COS Data Handbook*, Version 1.0 (Baltimore, STScI)
 Showman, A. P., Fortney, J. J., Lian, Y., et al. 2009, *ApJ*, 699, 564
 Snow, M., McClintock, W. E., & Woods, T. N. 2010, *Adv. Sp. Res.*, 46, 296
 Spiegel, D. S., Silverio, K., & Burrows, A. 2009, *ApJ*, 699, 1487
 Stone, J. M. & Proga, D. 2009, *ApJ*, 694, 205
 Tian, F., Toon, O. B., Pavlov, A. A., & De Sterck, H. 2005, *ApJ*, 621, 1049
 Trammell, G. B., Arras, P., & Li, Z.-Y. 2011, *ApJ*, 728, 152
 Trammell, G. B., Li, Z.-Y., & Arras, P. 2014, *ApJ*, 788, 161
 Tremblin, P. & Chiang, E. 2013, *MNRAS*, 428, 2565
 Vidal-Madjar, A., Lecavelier des Etangs, A., Désert, J.-M., Ballester, G. E., Ferlet, R., Hébrard, G., & Mayor, M. 2003, *Nature*, 442, 143
 Vidal-Madjar, A., Désert, J.-M., Lecavelier des Etangs, A., Hébrard, G., Ballester, G. E., Eherenreich, D., Ferlet, R., McConnell, J. C., Mayor, M., & Parkinson, C. D. 2004, *ApJ*, 604, L69
 Vidal-Madjar, A., Lecavelier des Etangs, A., Désert, J.-M., Ballester, G. E., Ferlet, R., Hébrard, G., & Mayor, M. 2008, *ApJ*, 676, L57
 Vidal-Madjar, A., Huitson, C. M., Bourrier, V., Désert, J.-M., Ballester, G., Lecavelier des Etangs, A., Sing, D. K., Eherenreich, D., Ferlet, R., Hébrard, G., & McConnell, J. C. 2013, *A&A*, 560, A54
 Visscher, C., Lodders, K., & Fegley, B. 2010, *ApJ*, 716, 1060
 Woods, T. N., Tobiska, W. K., Rottman, G. J., & Worden, J. R. 2000, *J. Geophys. Res.*, 105, 27215
 Yelle, R. V. 2004, *Icarus*, 170, 167